Star-Forming Structures in Perseus

Tom Laakso
Advisor: Prof. Alyssa Goodman

May 15th 2006

Abstract

This year, both the Spitzer c2d legacy project and the COMPLETE survey have released new infrared observations of Perseus. This new wealth of data has made possible a rigorous examination of star-forming processes in that region. We have unified Spitzer, CSO Bolocam, SCUBA and 2MASS observations of Perseus to create a "star-formation catalog" which contains: young stellar objects divided by infrared classification, gaseous cores, and extinction clumps. We present here several statistical studies of this catalog, including two-point correlations, nearest neighbor algorithms, and star-forming efficiencies.

1 Introduction

The basic mechanism of star-formation is the collapse of gaseous cores. Diffuse clouds of gas collapse under their own gravitational potential, and can fragment into smaller, dense cores, creating a hierarchicial density structure within the larger cloud. If the collapse continues, a central object will begin to form. Though it may still lack the critical mass necessary for fusion, further accretion onto this "protostar" releases a great deal of radiative energy. The radiation is absorbed by the surrounding halo of cold, optically thick dust, which then emits at its own characteristic wavelengths. The result is a spectral energy distribution (SED) shifted deep into the infrared, relative to a main sequence star; based on this energy profile, the dusty young object is given the label "class 0". Once enough mass has accreted onto the class 0 object, fusion intitiates and a star is born, shrouded into the remains of the core that birthed it (Carroll & Ostlie 1996). This envelope slowly thins out, falling inward through accretion and dissipating outward through turbulent motion. The remnants, due to angular momentum, flatten into a stellar disk. Thus the obscuring dust halo diminishes, and the SED of the object shifts blueward. As it progresses through this SED evolution, the young stellar object (YSO) is classified as class I, class II and then class III, before finally passing into the main sequence (Adams et al. 1997).

However, this is only a very general scheme. The specifics are still ill-understood. For example, the processes that initiate and end fragmentation remain largely unexplained. Formation in one region may, through the influence of outflows and gravitational perturbations, be able to trigger formation elsewhere, but this remains only a theory. The difficulty of determining three-dimensional motions and velocities also leaves us unsure how long stars remain associated with their parent cores.

Addressing these issues will require a better understanding of the hierarchicial struture of star-forming gas, and the distribution of young stars within it. However, until recently, observational data of star-forming regions was rather limited. With the recent advent of new infrared instruments, such as the Spitzer space telescope, and large bolometeric arrays like SCUBA (Submillimetre Common User Bolometer Array) and the Bolocam at Caltech Submillimeter Observatory, large-scale observations of these regions have become increasingly practical.

2006 has proved a milestone year for such observations. The Molecular Cores to Planet Forming Disks Spitzer Legacy Project released its Infrared Array Camera (IRAC) and Multiband Imaging Photometer (MIPS) surveys for young stellar objects in Perseus and Ophiuchus. 1.1mm and 850μm surveys of Perseus were also published, by Enoch et al. 2006 and Kirk et al. 2006, respectively.

Some analysis of the individual surveys has already been performed; core lists have been generated for the 1.1mm (Enoch et al. 2006) and 850μm (Kirk et al. 2006) lists, and a catalog of young stellar objects has been filtered from the Spitzer observations (Jorgensen et al. 2006). This paper, on the other hand,

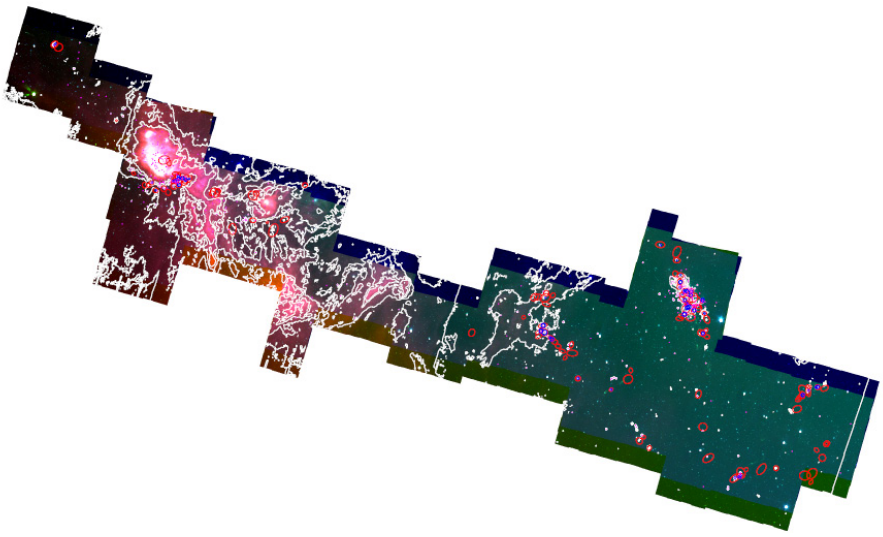

Figure 1: An overview of the data to be used in this paper. The background image overlays the integrated intensity from c2d observations in three bands, IRAC1 (3.6μm - blue), IRAC3 (4.5μm - green) and IRAC4 (8.0μm - red). Point sources identified as YSOs are plotted (pink boxes), as are contours of the MIPS1 (24μm) observations (white lines). Gaseous cores identified in the various COMPLETE survey are overlaid: 1.1mm (red ellipses), 850μm (blue circles).

will consider all of these catalogs *simultaneously*. The goal is to statistically assess the distribution properties of the young stars relative to the gaseous cores, and to hunt for correlations between their properties.

We set out to prove no specific hypothesis regarding star-formation in Perseus. However, by providing a quantitative analysis of star-forming structures, we hope to establish a conceptual and mathematical base for future investigation of some of the issues discussed above.

To this end, we present three statistical studies of the joint catalogs. §2 provides an introduction to the various data sets, and to the filtering processes used to create source lists from them. §3 addresses YSO clustering through the two-point correlation function. §4 considers the radial distribution of YSOs about the gaseous cores, as a function of YSO age. Finally, §5 calculates the efficiency with which cores convert their gas into stars.

2 Data

The goal of this paper is to study star-formation in Perseus through the distribution of its various components: young stars themselves, the remnants of the clouds which formed them, and cores of gas which are birthing new stars still.

In order to unite all of these objects, a great deal of observation is required, and thus this paper utilizes four different data sets.

1. IRAC observations, published by the Molecular Cores to Planet Forming Disks Spitzer legacy project team (Evans et al 2003). IRAC operates in four different bands, denoted by IRAC1 - IRAC4: 3.6μm, 4.5μm, 5.8μm and 8.0μm.
2. 1.1mm observations, taken using the Bolocam at Caltech Submillimeter Observatory, and published by Enoch et al., 2006.
3. 850μm observations taken using the Submillimetre Common User Bolometer Array (SCUBA) at the James Clerk Maxwell Telescope, and published by Kirk et al., 2006.
4. Extinction maps of Perseus processed from the 2-Micron All Sky Survey (2MASS) using the NICER algorithm, and published by the COMPLETE team (Ridge et al. 2006).

Both the 850μm and extinction data are part of the Coordinated Molecular Probe Line Extinction Thermal Emission (COMPLETE) survey of Star Forming Regions (Ridge et al. 2006).

2.1 Young Stellar Objects: Spitzer c2d

In order to produce a catalog of young stars in Perseus, we utilized data products from the Spitzer Cores to Disks legacy program. This section presents the Spitzer data, and discusses the filtering process used to create the final catalog of young stars.

The Molecular Cores to Planet Forming Disks Project (hereafter c2d) is a branch of the Spitzer Space Telescope Legacy Program. The goal of the c2d program is to produce observations that will follow the evolution of stellar systems from cores of gas to circumstellar disks. The observations are conduced in the IRAC and MIPS bands in order to observe dusty young star-forming regions (Evans et al.).

This paper uses the Third Data Delivery from the c2d project. This delivery covers five clouds in IRAC and MIPS, and includes a multi-band catalog of sources within the clouds. For details of the source extraction process, please refer to Harvey et al. 2005.

2.1.1 YSO Identification

For the purposes of this analysis, we wished to produce a list of young stellar objects (hereafter YSOs) in Perseus from the master list of IRAC and MIPS sources. Unfortunately, identifying stars as young can be a tricky process.

One method of identification is based on the spectral energy distribution (SED) of the star in question. Operating under the assumption that young stars are still embedded in the collapsing clouds from which they formed, the distribution of energies radiated from these stars will be dominated by the emission from accreting dust. These emissions are expected to be at longer wavelengths

than stellar emission itself, thus creating an "infrared excess" in the SED. Depending on the degree of excess, young objects are assigned a class; class 0 for the objects with heaviest infrared excess, through class III, with relative little excess. The class 0 objects are presumably deeply embedded, very young protostars, while the class III are pre-main sequence, but substantially older with only an optically thin disk remaining (Andre 1995).

However, obtaining full SED information for a large catalog of stars is a titanic undertaking. Much work has been, and is being, committed to finding a rigorous substitute for SED-based classifications. One possibility is the use of color-color spaces. Plotting objects of known infrared excess in various infrared, millimeter and submillimeter spaces indicates that sources of similar classification do have a tendency to cluster within these spaces. On the other hand, these clustering regions often overlap, and the boundaries show very different properties depending on which observing bands are used: any combination of J, K, L, IRAC1, IRAC2, IRAC3, and IRAC4 can conceivably be used. Furthermore, the inclination of the object can skew its color properties considerably, especially for the youngest sources (Whitney et al. 2003).

Based on the work of Jorgensen et al. 2006, we chose to define YSOs using use an IRAC color-magnitude space, [IRAC4] vs. [IRAC2]-[IRAC4]. This space was chosen due to the relatively clear age divisions it made in the SWIRE Elais N1 data. Based on the color-magnitude locations of non-star objects in the SWIRE observations, Jorgensen defined a color-magnitude cut most likely to eliminate reddened galaxies that might pose as young stars with infrared excess. A similar consideration of class III and main-sequence stars led to a second cut, intended to leave only the youngest objects. For a full discussion of how these criteria were generated from the SWIRE data, please refer to Jorgensen et al. 2006.

Before applying the color criteria, we eliminated some sources were for simler reasons. Sources which could be classified as "extended" (i.e., they had to be fit by ellipsoid in the Spitzer pipeline) were eliminated on suspicion of being redshifted galaxies. Furthermore, a source was only considered a true physical object if it produced a peak in all four of the IRAC bands.

A summary of the YSO filtering criteria is presented below:

1. sources must have A or B quality detections in all four IRAC bands: IRAC1 (3.6μm), IRAC2 (4.5μm), IRAC3 (5.8μm), and IRAC4 (8.0μm). (For the details detection quality flags, please refer to the c2d Third Delivery Release Document (Evans et al.).
2. Sources cannot have an ellipsoid fit, that is, they cannot be defined as extended.
3. The sources must obey the following color-magnitude criteria:
   [IRAC2]-[IRAC4]>0.5
   [IRAC4]>14-([IRAC2]-[IRAC4])

Figure 2 plots all objects which passed criteria 1 and 2 in the relevant color-magnitude space. The criterion 3 cuts are also plotted. The final YSO catalog

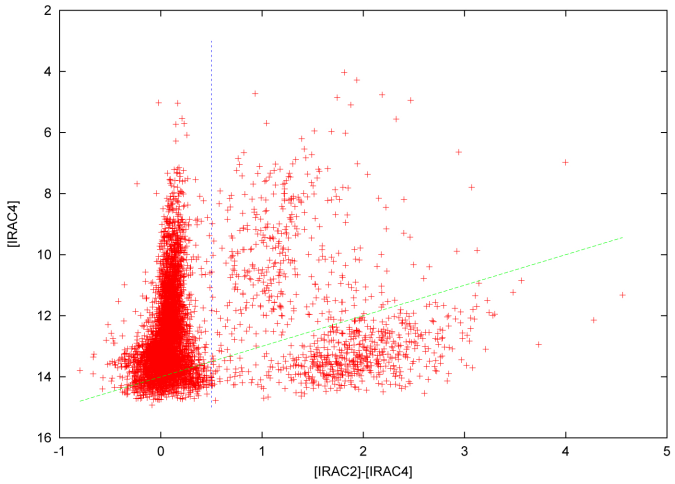

Figure 2: c2d sources with detections in all four bands and non-extended emission, plotted in an IRAC color-magnitude space. The two lines represent the final criteria for YSO status: objects must lie above the green line and to the right of the blue.

is displayed in figure 3 (top).

2.1.2 Completeness and Reliability of the YSO Catalog

What are the advantages and disadvantages of the filtering process described above? We can think about this in terms of completeness and reliability: does the data set contain a large percentage of all actual YSOs (is it complete) and does it contain minimal objects which are not actual YSOs (it is reliable)? We'll consider this on a criterion-by-criterion basis.

The first criterion is intended to prevent false detections from entering the catalog by assuming that real sources will emit in all four IRAC bands. While this rule makes it likely that any included source *will* reflect a real physical object, the four-band emission requirement probably causes a rejection of some of the youngest stars. Class 0 objects are defined as having minimal emission at wavelengths shorter than 10μm (Andre 1995), so there is little reason to expect these important objects to be detected in the IRAC1 band, centered on 3.6μm. Thus, this criterion encourages reliability at the expense of completeness.

The second criterion is meant to prevent reddened galaxies from being included in the YSO catalog. Unfortunately, as pre/early stellar objects may have very extended emission due to their still large associated dust clouds, this criterion may also exclude some of the youngest sources in the name of catalog quality. An example of the completeness problem is demonstrated by the case of L1448, presented in figure 4.

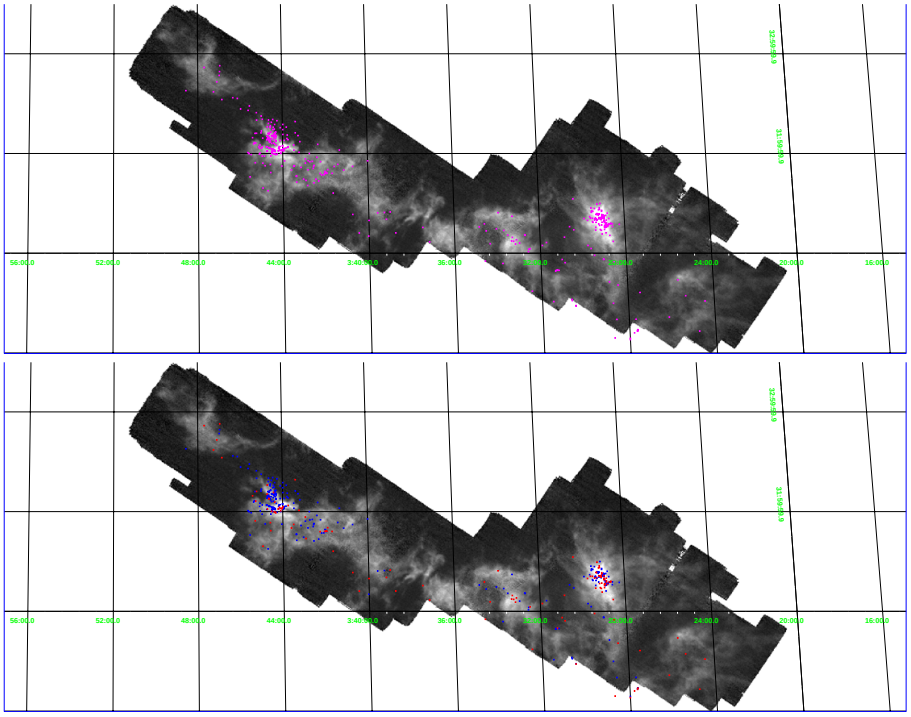

Figure 3: The YSO source list produced by filtering the c2d 3rd delivery. For reference, integrated ^{13}CO emission is used as a background image. Top: YSOs. Bottom: YSOs divided by infrared excess classification; class I (red) and class II (blue). The dense cluster on the left is composed mostly of main sequence objects; the thinner cluster in the lower right is mosly likely an assortment of reddened galaxies.

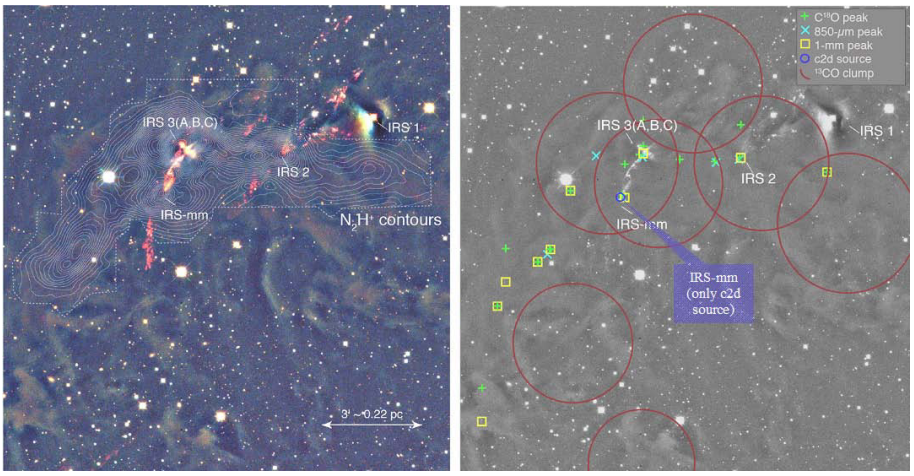

Figure 4: Completeness vs. reliability: L1448. These are two infrared images of L1448 (Foster & Goodman 2006); the left is presented in color to enhance certain features, while the right is in grey scale to allow the overplotting of several sources. Despite the presence of multiple outflows (visible on the left), a number of emission peaks in multiple bands (plotted on the right; a number conspicuously coincide), only one YSO from the filtered list appears in the region. While the strict filtering criteria make the YSO catalog reliable, it is very evidently incomplete.

The third criterion, based on actual observations of both pre-main sequence and main sequence stars, as well as redshifted galaxies, seems to be of solid repute. However, the uncertainties in color-color (or color-magnitude) diagrams, as discussed in §2.1.1, casts some doubt on any YSO identifications not based on strict SED analysis. It is difficult at this time to determine what selection effects these color-restrictions may have imposed on the data set; further study is required.

In summary, the filtering criteria have created a YSO set that is reliable, though at the expense of completeness. At this early stage of study, reliability provides us with a firm footing to take a first step in the analysis of c2d data; further study can build on this work once a more complete YSO catalog has been generated. However, the catalog does retain some uncertainty: the precise effects of the color-magnitude criteria are still undefined. For the purposes of this analysis we will generally assume that those effects are minimal, but some skepticism here would certainly be healthy.

2.1.3 Class I and Class II Filters

In addition to identifying the YSOs, we have made an attempt to divide them by class. Divisions were made based on color-color criteria derived in Allen et al. 2004. Those criteria are as follows (note that this assumes class III and main sequence stars have alread been omitted by the intial YSO filters):

Class I: [IRAC1]-[IRAC2]$>$0.7 or [IRAC3]-[IRAC4]$>$1.0
Class II : [IRAC1]-[IRAC2]$\leq$0.7 and [IRAC3]-[IRAC4]$\leq$1.0 and [IRAC3]-[IRAC4]$>$0.4

The sources are plotted in the relevant color-color space in figure 5. Figure (bottom) displays the source-divided catalog as it appears in the sky.

As discussed in §2.1.1, the use of color-color criteria as a substitute for full SED analysis of infrared excesses is a highly active and evolving field. It is still unclear at this point how reliable the color-color criteria applied here actually are. As with any color-color space, the boundaries between classes are somewhat blurred (Allen et al. 2004), and effects such as inclination can have serious effects on the color properties of an object (Whitney et al. 2003). Therefore, full confidence in the class I/II designations is simply not possible at this time. As with the full YSO catalog, some skepticism of the infrared excess classifications will prove healthy.

Clearly the various uncertainties in our YSO source list, and in age classifications within that list, must be kept in mind when performing any analysis; thus, this paper will refer frequently to these issues under the umbrella term of "filtering criteria".

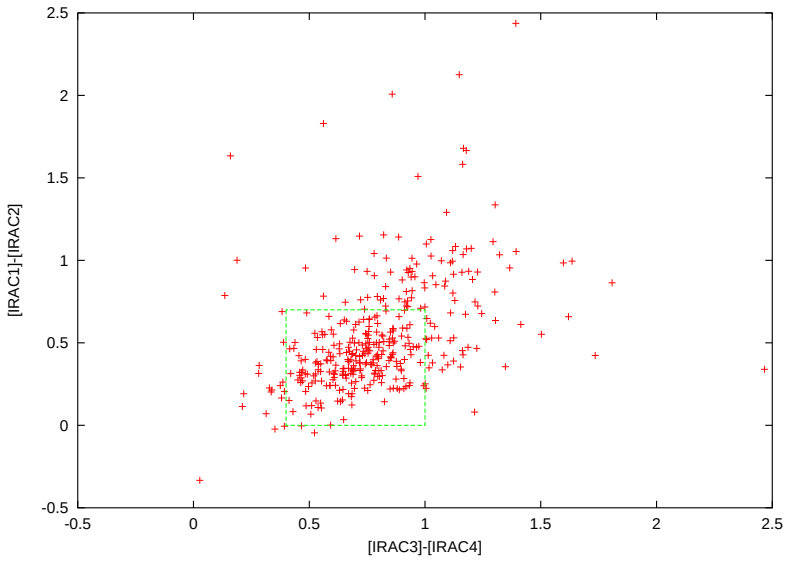

Figure 5: YSOs, plotted in an IRAC color space. All sources falling within the green box are identified as class II; sources above or to the right of the box are identified as class I. Other sources are not given an infrared excess designation.

2.2 Gaseous Cores: 1.1mm and 850μm Emission, and 2μm Extintion

Stars forms in dense condensations of gas; but what emission mechanism best traces the regions which are actively involved in star-forming? Generally, one can expect millimeter and submillimeter emission to act as a respectable tracer: the dusty cores which collapse to form protostars, and the residual envelopes carried by class 0 and class I stars emit heavily at these frequencies. The dust is optically thin to this emission, so the sub/millimeter emission is a reliable tracer not just of core location, but of core mass.

Fortunately, the abundance of data now available for Perseus allows us to analyze the cloud at multiple wavelengths. Here we use 1.1mm and 850μm data to trace the cores themselves, as well as 2μm extinction to identify large-scale structures.

2.2.1 1.1mm Emission

This data comes from the work of Enoch et al. 2006. The data was taken using the Bolocam at Caltech Submillimeter Observatory, with survey bounds following the c2d observations in order to cover a 7.5 deg^2 area. The survey was conducted with an effective beam size (full-width half max, if approximated as gaussian) of 31". From this data, 122 emission peaks were identified. Peaks are defined as point-sources that are more than 5 σ above the rms noise, where 1 σ rms = 15 mJy beam^{-1}. The peak can be thought of as associated with a gaseous core based on major and minor axes centered on the emission peak; these axes are the full-width half-maxima of a gaussian fit to the integrated emission profile. For further details of the source-identification process, please refer to Enoch et al. 2006.

The 1.1mm cores are plotted on a ^{13}CO map of Perseus in figure 6.

2.2.2 850μm Emission

This data comes from the work of Kirk et al. 2006. The observations were taken at the James Clerk Maxwell Telescope as part of the COMPLETE project, using the Submillimetre Common User Bolometer Array (SCUBA). The survey bounds define a region of 3.5 deg^2, observed with an effective beam size (full-width half max, if approximated as gaussian) of 19.9" This data was used to identify 49 cores. These cores are defined around emission peaks that are greater than 3 times the rms pixel noise. Effective radii for the cores are based on the two-dimensional Clumpfind algorithm (Williams et al. 1994). For a more detailed discussion of the source-identification process, please refer to Kirk et al. 2006.

The 850μm cores are plotted on a ^{13}CO map of Perseus in figure 6.

2.2.3 1.1mm vs. 850μm: A Comparison

While identifying YSOs is a complicated business, defining cores of gas is even more fraught with difficulties. First, the different surveys were conducted from different telescopes, and at different wavelengths, which results in different beam sizes. The 1.1mm survey was conducted with a beam of 31", the 850μm with a beam of 19.9". This difference means that the 850μm survey can pick out smaller structure, due to their higher resolution.
Furthermore, due to observational technique, the SCUBA survey is less sensitive to large structures than the CSO Bolocam survey. The former used chopping, with throws of 33" and 44". This method tends to cause a loss of sensitivity for objects substantially larger than the throw. The Bolocam observations, on the other hand, were conducted without chops, thus allowing sensitivity to structure up to the full angular size of the array, 7.5'. This accounts for some of the statistical differences in the surveys; most notably, the difference in average core radius: 30" for the SCUBA data, and 70" for the Bolocam data.

Finally, the two surveys have different detection threshholds; the 1.1mm survey is sensitive to clumps with masses down to 0.2 $M_{\odot}$, while the 850μm survey is sensitive to about 0.3 $M_{\odot}$. However, relatively few clumps fall in this range in the Enoch survey, so the sensitivity limits should not be a substantial source of disagreement between the two core catalogs.

Once observations of emission have been obtained, one still faces the troublesome task of determing what exactly defines a "core". Such choices can have pronounced effects on the statistics of the core catalog that is ultimately produced.

Thus, it should be noted that the two surveys, in addition to observing at different wavelengths, define structure in very different ways. The 1.1mm definition is based on gaussian fitting of local peaks, while the 850mum is based on the Clumpfind algorithm. These distinctions results in differences in the number of cores identified, as well as in core properties such as size, mass, etc. As with the YSOs, these definitions will be critical to a proper analysis of the data.

2.2.4 2μm Extinction

Extinction mapping, based on 2MASS observations of the Perseus region, allows for a relatively low-resolution, large-scale map, and can thus be used to understand the cloud's biggest structures.

As part of the COMPLETE project, the NICER algorithm (Lombardi & Alves 2001) has been applied to portions of the 2MASS data to produce such maps. Coverage was chosen to correspond to the c2d observations, and to include any region with A_V >5, as well as most regions with A_V >3 (Ridge et al. 2006). Giant extinction "clumps" were then identified by further smoothing the data to a 5' resolution, and applying the corefind algorithm (Kirk et al. 2006). The resulting 11 clumps have an average radius of almost 3'.

The 2μm extinction clumps are plotted on a ^{13}CO map of Perseus in figure 6.

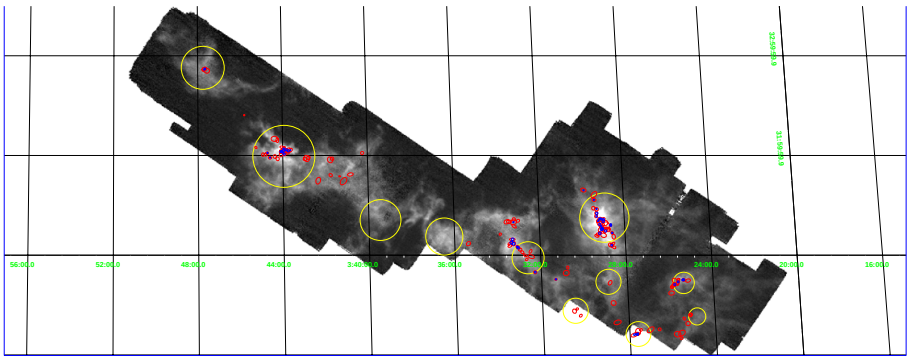

Figure 6: Gaseous cores in Persus, including 1.1mm cores (red ellipses), 850μm cores (blue circles) and 2μm extinction clumps. (yellow circles). The background is an integrated intensity map of ^{13}CO, also part of the COMPLETE survey.

3 The Two-Point Correlation of YSOs

A simple first step toward understanding the star-forming structures underlying Perseus is to measure the clustering of YSOs relative to a random distribution of stars. Later sections with consider YSO distribution around the cores, but a measure of YSO clustering independent of the gas will provide the clearest answers to simple but vital questions such as: are the YSOs clustered, and to what degree? Do different regions of Perseus exhibit different clustering behaviors? Do different classes of YSOs exhibit different behaviors?

Visually, the YSOs clearly cluster (see figure 3). However, we wish to quantify the degree of this clustering. There are any number of statistical measures available; we have chosen to use a measure often utilized in cosmological studies, the two-point correlation function.

3.1 Two-point Theory and Methods

The angular two-point correlation function, $w(\theta)$, is a measure of the *overdensity* of a distribution of objects, in excess of the density of a random distribution. To be a bit more rigorous: given a point-source catalog with mean number density n, w is defined by

$$\delta P(1,2) = n^2 \delta V_1 \delta V_2 [1 + w(\theta_{12})] \tag{1}$$

where δP is the joint probability of finding an object in both of the infintesimal volume elements δV_1 and δV_2, which have an angular separation of θ_{12}.

A more intuitive definition comes from considering the conditional probability of finding an object in volume δV_1, given that an object has been found in element δV_2 with probability nV_2:

$$\delta P(1|2) = n \delta V_1 [1 + w(\theta_{12})] \tag{2}$$

Because δV_2 is an arbitrarily chosen volume, it is permissible to drop the subscripts and interpret (2) as the probability that a given object has a neighbor at an angular separation of θ. (Peebles 1980).

With this interpretation in hand, consider a totally random, Poison-process catalog of sources. The probability of finding a neighbor at any arbitrary distance is simply $n^2\delta V_1\delta V_2$; therefore, $w(\theta)$ will be zero for all θ. However, if the probability of finding a neighbor in the volume element is greater than the mean, w must become positive. It is in this sense that the two-point correlation is a measure of *overdensity*; it increases with increasing source clustering.

Calculating w from this definition would clearly be very difficult. Generally, therefore, the two-point correlation is calculated using an *estimator*. For the purposes of this analysis, we use the basic estimator

$$1 + w(\theta) = \frac{H_D(\theta)}{H_R(\theta)} \tag{3}$$

where $H(\theta)$ is a the number of source pairs with separation θ. H_D considers pairs within the data set, while H_R counts pairs within an artificial catalog. This artifical catalog contains sources with random spatial distribution, though it maintains the selection effects and mean density of the physical catalog. This estimator is computationally simple, and has a nearly Poisson variance (Landy & Szalay 1993). More complex estimators do exist, many involving correlations between the random and physical catalogs; for a discussion of the virtues and weaknesses of those methods, see Landy & Szalay 1993.

The random catalogs were created through a monte carlo process, spatially limited by the observing bounds of the c2d survey. After applying this data to the estimator, we found that a power law of the form $w(\theta) = k\theta^\gamma$ provided a good fit to data points tha fell between the scale of the 850μm cores and the extinction clumps. The choice of a power law based on its use in cosmological studies, where power laws have proved excellent fits for cosmological-scale clustering (Peebles 1973).

3.2 Two-point Results and Analysis

3.2.1 Two-point Correlation of All YSOs

The calculation of $w(\theta)$ for all YSOs in Perseus is presented in figure 7. The young sources show positive correlation for angular separations of up to $0.2°$. Note that the average radius of the extinction clumps, weighted by the number of stars they contain, is R_{ext}=0.19°. This similarity suggests that regions of high extinction may coincide with regions of heavy YSO clustering - *if we assume that the peaks of extinction are the centers of clustering.* A visual examination of the most heavily populated extinction clumps (which will dominate calculations of both w and R_{ext} confirms that this is roughly the case; see figure 8. Could extinction indeed be acting as a strong bound on clustering in IC 348 and NGC 1333? This is a worth considering. The clustering itself is mostly likely an indicator of proximity to an active group of star-forming cores; thus, a w/A_V

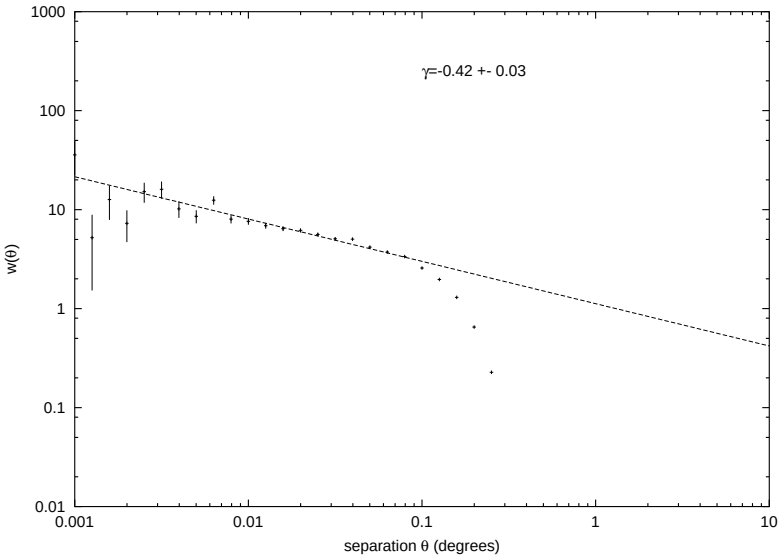

Figure 7: The two-point correlation function for all YSOs in Perseus. Errors are $N^{\frac{1}{2}}$. The fit is a power-law of the form $w = k\theta^{\gamma}$, based on the points $0.003^{\circ} < \theta \leq 0.1^{\circ}$

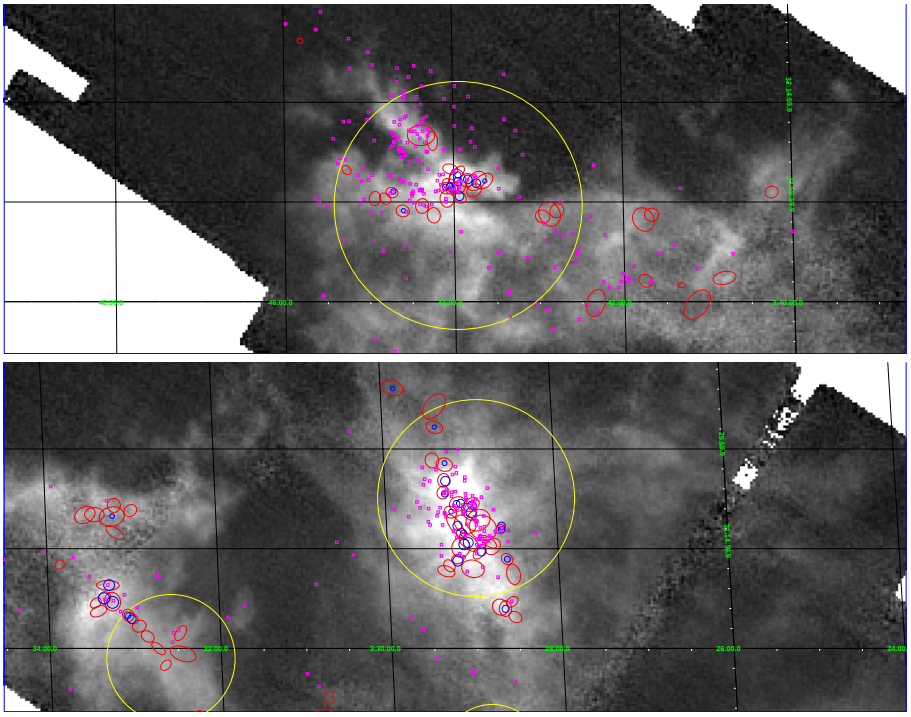

Figure 8: The clustering of YSOs (magenta boxes) in IC 348 (top) and NGC 1333 (bottom). Extinction clumps are shown in yellow. 1.1mm peaks (red) and 850um peaks (blue) are also shown. Note that the YSOs cluster around the center of NGC 1333 extinction clump. The overall distribution of IC 348 sources is centered somewhat north and east of the local extinction clump's center, but is still well within the boundary.

correlation would suggest that the 2μm extinction acts as a strong selector for the star-forming regions, even though it is not used to detect the formative cores themselves. This agrees with the work of Kirk et al. 2006, who argue that star-formation occurs only in high-extinction; the correlation is not an observational bias. They suggest A_V=5 as a lower extinction limit for star formation.

In order to check for this correlation more closely, two-point correlations were calculated for those regions. The results are presented in figure 9. Based on these plots, clustering terminates at 0.25° for IC 348 and 0.2° for NGC 1333. For comparison, the radii of the extinction clumps are 0.31° and 0.25°, respectively. Therefore, the extinction clumps can only be considered upper bounds on the absolute clustering radius of the heavily-populated cores. (Though not totally unreasonable bounds!) Unfortunately, too few points are available to rigorously estimate the two-point correlation in the smaller sub-regions.

3.2.2 Two-Point Correlation by Infrared Classification

Figure 10 presents the two-point correlation for class I and class II sources in all of Perseus. Though the errors are quite large for very small separations, power-law fits could be made in the range 0.01°-0.1°. (For comparison, 0.01°=36" is an average radial size for an 850μ core, while 0.1°=3600" is an average radial size for an extinction clump.) On these scales, the two classes show substantially different clustering behavior: class I objects have a significantly steeper drop in correlation than their class II fellows. This suggests that the younger sources are in more compact clusters than the older sources. To be more precise, as you move away from a source, the probability of finding a neighboring source of the same class source decreases at a faster *rate* for class I sources than for class II sources. Furthermore, there is a higher *absolute* probability of finding a class I source very close to another class I source, than is the case for class II objects. These relationships can be grasped qualitatively by simple maps of the stars; see Figure 11.

To put all these exponentials factors in context, consider a very simple, "toy" model of star-formation. In this world stars form out of totally static gas cores, but, due to the influence of local objects, these new stars gain some velocity relative to the core. Though the static core assumption is a bit unreasonable, we *do* expect to see random motions among YSOs that originated in the same region. This may be the result of ejection from a multiple star system, or due to purely random motions. See, for example, Kiseleva et al. 1998, Goodman & Arce 2004. Assuming there is a spread of just a few kilometers per second in the speeds, then the stars will disperse into a loose cloud of sources around the core. The younger a star, the closer it will be to the central core, within the constraints imposed by the spread in velocities. These younger sources will therefore also be, on average, closer to each other than older sources will be, with a density that falls off rapidly as one moves away from the core [1].

[1] Up to this point, interpretation of the two-point correlation function has all been based on two-dimensional observations of the sky. This may lead to some confusion; after all, sources are actually distributed in three dimensions, and it is unclear how meaningful it is to talk

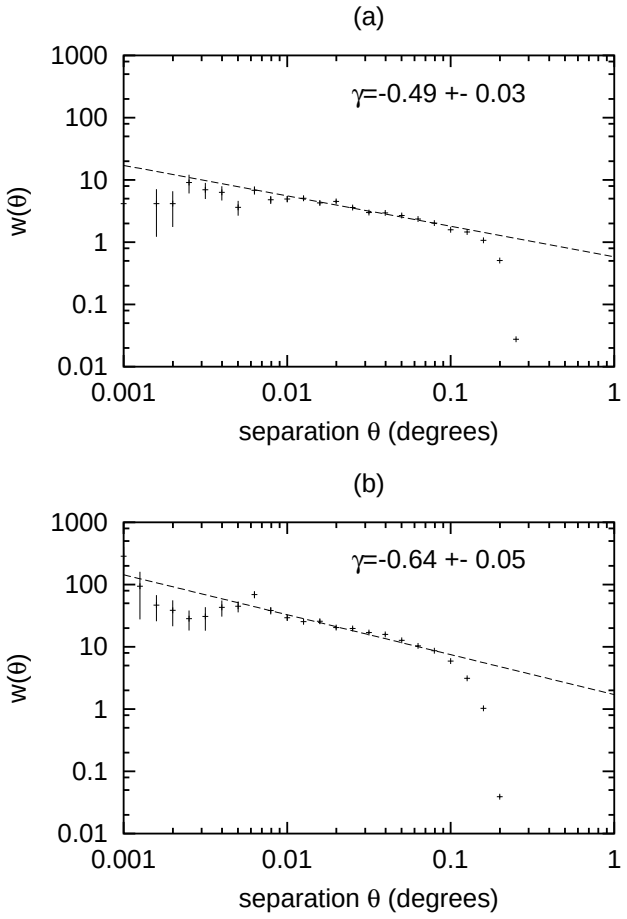

Figure 9: The two-point correlation function for YSOs in: a)IC 348, b) NGC 1333. Errors are $N^{\frac{1}{2}}$. Fits are power-laws of the form $w = k\theta^{\gamma}$, based on the points: a) $0.008^{\circ} < \theta < 0.16^{\circ}$, b) $0.008^{\circ} < \theta \leq 0.1^{\circ}$.

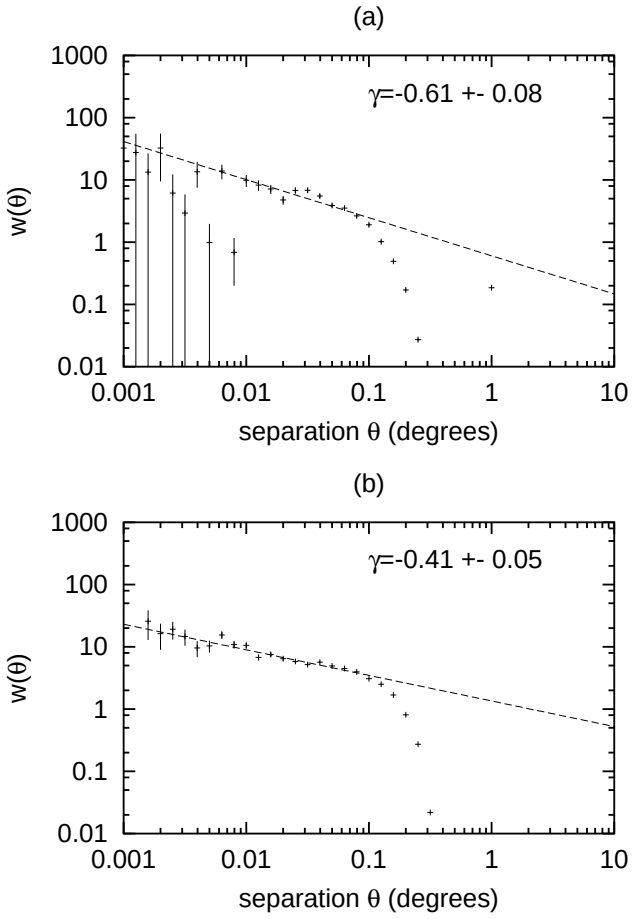

Figure 10: The two-point correlation function across all of Perseus for: a) class I sources, b) class II sources. Errors are $N^{\frac{1}{2}}$. Fits are power-laws of the form $w = k\theta^{\gamma}$, based on the points: a) $0.01^{\circ} < \theta \leq 0.1^{\circ}$, b) $0.005^{\circ} < \theta \leq 0.1^{\circ}$.

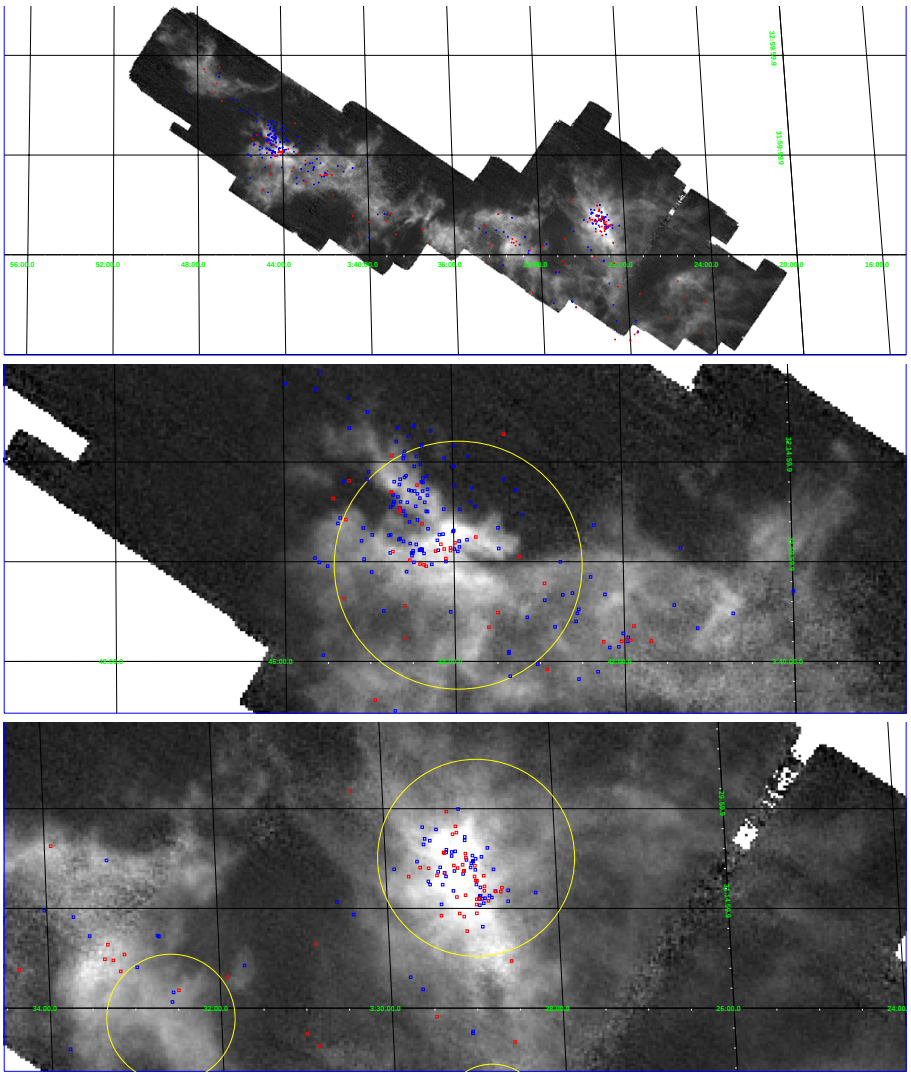

Figure 11: A visual comparison of class I (red) and class II (blue) sources in Perseus (top), IC 348 (middle) and NGC 1333 (bottom). For purposes of orientation, ^{13}CO integrated intensity (gray scale) and extinction clump boundaries (yellow) have been included. While the two-point correlation reveals important differences in clustering properties, the distinctions can be difficult to identify by eye. The tighter clustering of class I sources is clearly apparent in NGC 1333, but less obvious in IC 348.

This toy model accounts for the major features seen in the real two-point correlation functions:

1. The youngest sources are closer to each other than is the case with the older sources. Therefore, the excess probability of finding a neighbor at small separations is greater for class I sources than for class II sources.
2. The spatial distribution of the young sources is tighter than that of the older sources. Therefore, the class I probability of a finding a neighbor should, as a function of increasing separation, drop more quickly than the equivalent class II probability. Hence, $\gamma_I < \gamma_{II}$.

However, the two-point results must be kept in proper context. There is a definite possibility that the source lists are not accurate reflections of the age distributions of stars, making the estimates of w by class dubious at best. Sources of suspicion are two-fold.

First, young objects, the youngest class I sources in particular, may have been filtered out of the source lists. As discussed in §2.1, there is a pair of reasons for such an exclusion: first, the youngest objects have extended envelopes. The resulting large angular span may have tricked our filtering algorithm into classifying them as galaxies. Second, the highly reddened SEDs of the youngest YSOs are unlikely to produce an emission peak in all four IRAC bands. The filtering algorithm identifies any object which does not peak in all 4 bands as a false detection. At this time, it is not clear what the probability function is for positive selection of a source as a function of its SED or color properties. Therefore, it is not possible to say if the rejected objects fall across the range of class I sources, or are clustered mainly at the youngest end. In the former case, inclusion of these objects might not have much effect on w, other than to decrease the errors; in the latter case, inclusion of very young, and therefore probably very clustered objects might result in a substantial drop in the value

about source motions when we only have information on the *projection* of those motions onto the sky. While we cannot rigorously calculate the a spatial two-point correlation $\xi(r)$ without measurement of the distances to all the stars, it is possible to mathematically extrapolate the form of ξ from the angular function, w:

$$w(\theta) = A\theta^{\gamma}$$
$$\xi(r) = B(\gamma, A) r^{\gamma - 1}$$

B is a complicated function defined in terms of the Mellin transform, and is not very enlightening. However, the basic form of the correlation is easy to grasp. It is also a power law, though the exponent will be more negative than in the 2-D case. The class I/class II exponents will also be closer to one another:

$$\frac{\gamma_I}{\gamma_{II}} = 1.48$$
$$\frac{\gamma_I - 1}{\gamma_{II} - 1} = 1.14$$

This suggests that the projection effects tend to over-emphasize the difference between the two age classes. However, there is still a 10% difference in the ratio of the γs, so the qualitative discussion of the 2-D distributions should hold in the 3-D case as well.

of γ_I.

The second cause for skepticism is the procedure used to define "class I" and "class II". While age determination by IRAC color is a very active field, the question of the best procedure to use is still being debated. The criteria used here (Allen et al. 2004) seem quite powerful, but the boundary region between class I and class II is slightly blurry, a potentially critical distinction when considering a few tens of stars; a small shift in the color-color boundaries could switch the classifications of a large percentage of the sources. Indeed, these particular criteria may or may not prove to be the best possible rules among the host that are being considered. The work of Whitney et al. 2003 found that color-color identifications of the different stellar evolutionary states are skewed by the inclinations of stellar disks, perhaps severely. This problem is reduced by using far-infrared MIPS bands. A MIPS color-magnitude analysis of the YSOs appears to be an especially promising line of inquiry.

Thus, while the IRAC-based class I/II catalogs assembled here serve as a good starting point, any calculation based on them must contain some additional intrinsic uncertainty.

age group	region	γ	$r_{w\to 0}$		core type	average radius
all	Perseus	-0.42±0.03	720		1mm	70
all	IC 348	-0.49±0.03	900		850μm	60
all	NGC 1333	-0.64±0.05	720		2μm extinction	680
class I	Perseus	-0.61±0.08	900			
class II	Perseus	-0.41±0.05	1080			

Table 1: A summary of YSO two-point correlations in Perseus, including:
1. the exponential factor γ from power law fitting of w,
2. the *approximate* radius at which w vanishes
For comparison, the average radii of the various cores are also listed here. All radii are given in arcseconds.

In summary, the YSOs in Perseus cluster with an overdensity that runs like a power law with exponential parameter γ=-0.43. Furthermore, in regions with high YSO-population, namely IC 348 and NGC 1333, the extinction clumps serve as respectable outer bounds on regions of clustering. Finally, class I objects in Perseus appear to show substantive clustering compared to class II objects: γ_I=-0.61, γ_{II}=-0.44. Uncertainty in the definitions of YSO and class I/II, however, make this last result questionable. §4.1 will attempt to address some of this uncertainty by looking at clustering properties of stars as a function of their color, without assigning classifications.

4 Core Associations and YSO Color

Section 3 considered the absolute spatial distribution of the YSOs. We now wish to introduce the gaseous cores in which these stars formed, and analyze

the relationship between star and cloud. Thus, this section will consider both the spatial distribution of YSOs relative to the gaseous cores in Perseus (§4.1), as well as any correlations between the properties of stars and their formative clouds (§4.1).

For such an analysis to be meaningful, we need to determine which star originated in which cloud. The easiest way to do this is to consider a star's "mother" core to be the core it is closest to, its nearest neighbor. Of course, for tightly clustered cores, or for stars with even moderate random motions, this may not be a sound assumption. Indeed, many of the cores in the survery ARE tightly clustered, and a number of studies have shown that young stars have random motions on the order of a few kilometers per second (for example, Frink et al. 1997, Goodman & Arce 2004). However, nearest neighbor assignation it is the best we can do; determining the velocity of individual stars is far beyond the scope of this paper.

4.1 YSO Color Parameter vs. Nearest Core Distance

Analysis of the two-point correlation (see §3.2) has, not surprisingly, suggested that younger stars in Perseus cluster more tightly than their older relatives. This section will also consider star clustering by age; however, it will introduce further complexity by measuring YSO distribution relative to the gaseous cores of Perseus.

There are a number of ways to measure spatial distributions of two objects relative to each other; for simplicity, we have chosen to use the separation between a YSO and its nearest core-neighbor. Once again in the name of simplicity, the perilous color-based age classifications discussed in §2.2 have been abandoned in favor of the IRAC colors themselves. In addition to dodging the bullet of that method's uncertainty, direct use of color parameters allows a finer differentiation than is permitted by the use of an either/or distinction between classes I and II.

Figure 12 presents the basic results. Each YSO was associated with a nearest 1.1mm and 850μm core. Distances are measured to the emission peak, which is the core's center. A pair of color parameters was then calculated for each YSO; these parameters were chosen to coincide with those used in Allen et al. 2004. Color parameter was then plotted against core distance, for each of the four possible combinations.

A visual examination of the data reveals an interesting difference in the radial distributions of the two colors. Note that the [3.6μm]-[4.5μm] space contains a tail of YSOs that swings to very high y-axis values (very red emission) at very low x-axis values (very nearby core). This tail indicates that the YSOs with the most reddened emission in this color are clustering close to both the 1.1mm and 850μm cores. The lack of such a distinct tail in the [5.8μm]-[8.0μm] space means that this color is distributed more or less uniformly with radial separation from nearest core. The existence of outlying sources in the [3.6μm]-[4.5μm] parameter agrees with Allen et al. (2004), who found that class I and II sources, when plotted in the [3.6μm]-[4.5μm] vs. [5.6μm]-[8.0μm] color space,

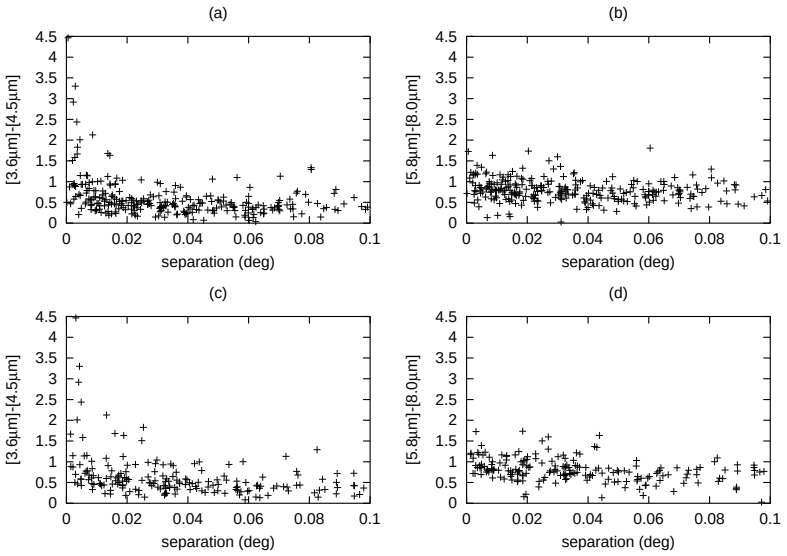

Figure 12: YSO Color differences (in magnitudes) vs. separation from nearest core. a),b) Distances are to 1.1mm cores. c),d) Distances are to 850μm cores.

showed substantially more spread in the y-direction than the x. In summary, the reddest, and presumably youngest, sources are clustering around gaseous cores. This is precisely as we would expect from the toy model of star-formation discussed in §3.2.

In order to quantify the degree of clustering present, we chose to impose a fit on the data. A power law proved to be the best choice. For comparison, a fit was also imposed on a randomized data set, in which the flux and colors of each star in the catalog was reassigned an arbitrary position within the bounds of the c2d survey. The physical data and the random data were fit in identical fashions. These fits are displayed in figure 13.

The resulting fits for the 1.1mm and 850μm data correspond with the given uncertainties. Furthermore, both show substantial deviation from the random data. This suggests that the YSO distribution *by color* is similarly structured around both types of core. While this is gratifying, a blind faith in the power law fits can obscure some fine distinctions between the two data sets. Based on a human-eye check, the reddened tail of the 1.1mm data appears to be tighter than that produced by the 850μ survey. Prompted by this, we can consider only the most reddened 10% of the YSOs: their average separation from the nearest 1.1mm core is 290", while their average separation from the nearest 850μm core is 550", almost twice the angular distance! The two emissions types must be tracing phenomonologically different regions of the gas, with the 1.1mm emission peaks more closely reflecting loci of dusty red YSOs.

4.2 YSO Color Parameter vs. Nearest Neighbor Properties

If the 1.1mm/850μm cores are indeed centers of clustering for the youngest, reddest stars - and therefore their likely birthplaces - one might wish to ask how the core properties correlate with the age of their offspring. Thanks to the wealth of the COMPLETE data, it is possible to plot YSO colors against the mass, area, peak luminosity, and local 2MASS extinction of their nearest core neighbors.

Results are presented in figures 14-17. The red line in these plots denotes the lower limit of the reddest 10% of YSOs, in the relevant color space. None of these relations appear to yield any correlation; automated fitting algorithms yield high errors on all fit parametrs. The reddest 10% of objects are distributed quite widely across the range of neighboring core parameters.

Though a negative result, it is still of interest that neither the size/mass, luminosity nor extinction of a core affects the color of the young stars it harbors. Since the color of a star reflect their age, which reflects the age (since collapse) of the core that formed it, we can state that we cannot determine the age of core based on its other physical properties.

The lack of an extinction correlation is a bit puzzling. In areas of high extinction, one might expect to find the densest gas regions; as possible products of gravitational collapse, such regions would most likely play host to a number of the youngest stars. This seems even more puzzling given that, indeed, cores

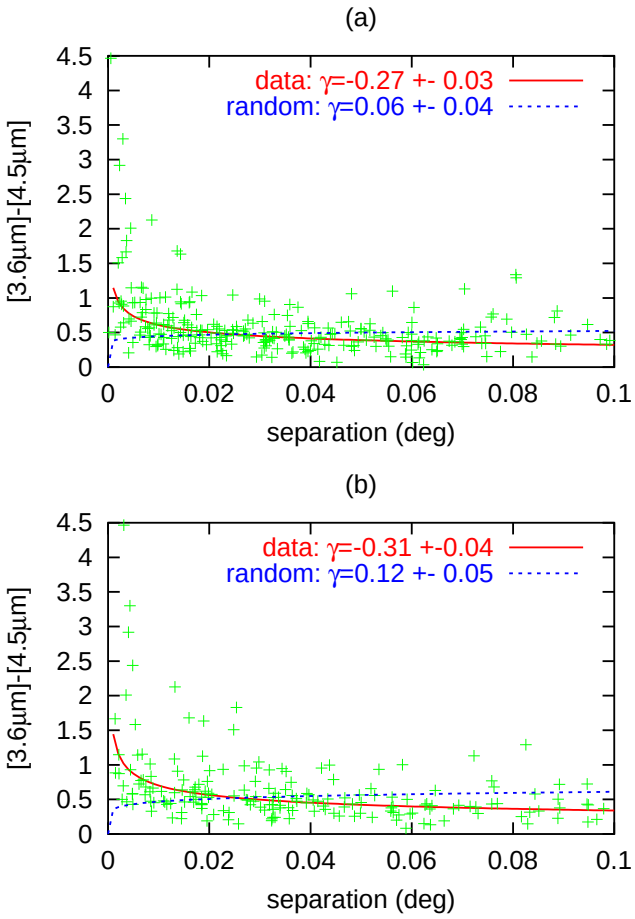

Figure 13: [IRAC1]-[IRAC2] for the YSOs vs. separation from nearest core. a) Distances are to 1.1mm cores. b) Distances are to 850μm cores. A power law (solid red) fit has been applied to the data. For comparison, a second power law fit (dashed blue) has been applied to a randomized data set (not shown).

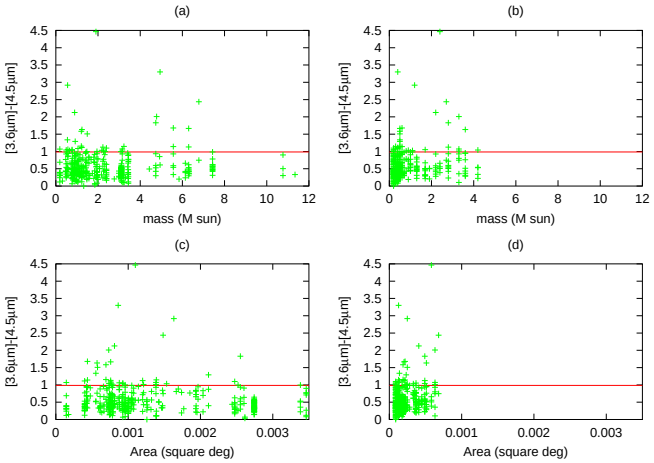

Figure 14: YSO colors vs. properties of nearest neighboring core: [IRAC1]-[IRAC2] vs. a) 1.1mm mass, b)850μm mass, c)1.1mm area, d)850μm area.

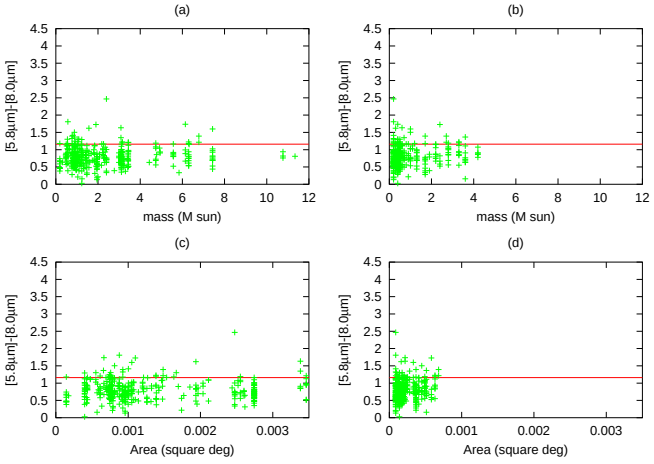

Figure 15: YSO colors vs. properties of nearest neighboring core: [IRAC3]-[IRAC4] vs. a) 1.1mm mass, b)850μm mass, c)1.1mm area, d)850μm area.

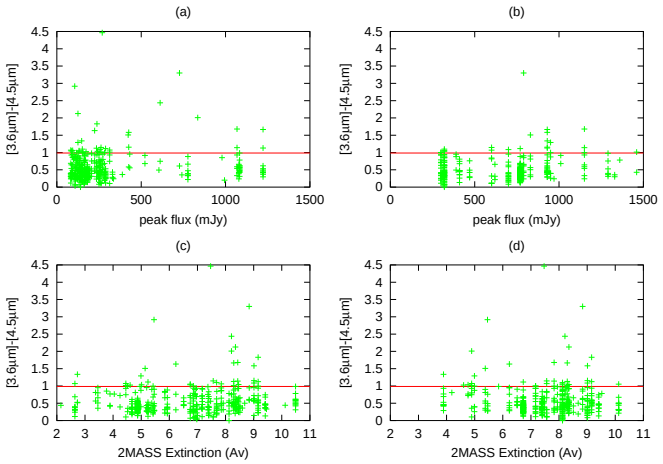

Figure 16: YSO colors vs. properties of nearest neighboring core: [IRAC1]-[IRAC2] vs. a) 1.1mm peak flux, b)850um peak flux, c)2MASS extinction local to 1.1mm core, d)2MASS extinction local to 850um core.

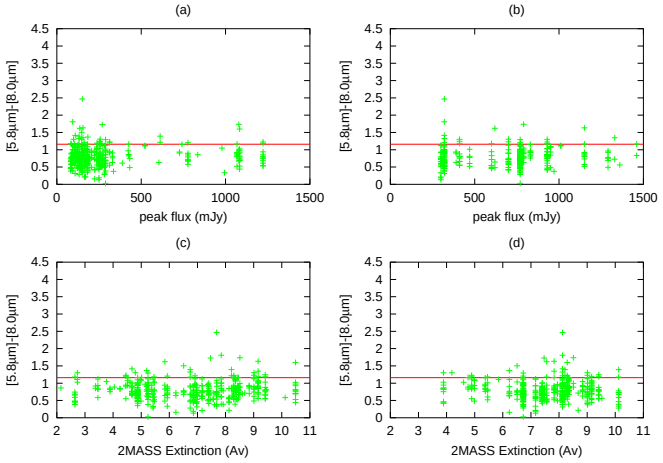

Figure 17: YSO colors vs. properties of nearest neighboring core: [IRAC3]-[IRAC4] vs. a) 1.1mm peak flux, b)850um peak flux, c)2MASS extinction local to 1.1mm core, d)2MASS extinction local to 850um core.

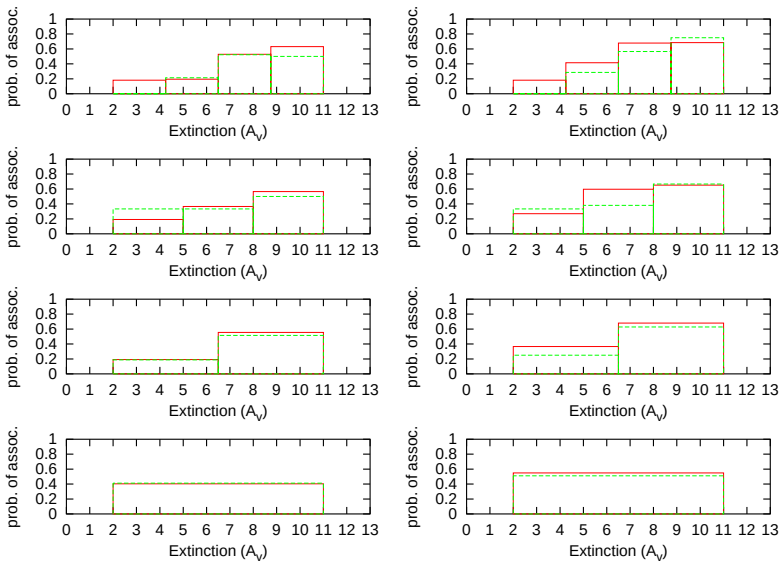

Figure 18: The probability of finding a YSO associated with a 1.1mm core (red) or 850μm core (green), as a function of the core's associated 2MASS extinction. Association is defined as: a) the YSO is located within the boundary of the core. b) the YSO is located with 1.5x the boundary of the core. Note that the probability increases substantially for higher extinction.

with high associated 2MASS extinction are the most likely to have an associated YSO of any age; see figure 18.

The lack of a correlation may be explicable through the YSO filtering criteria(see §2.2), which probably may removed the reddest, youngest stars from the catalog. If this is the case, the plots in figures 16 and 17 might be missing critical points at high reddening and high extinction, despite the increased probability of finding *some* YSO at higher extinctions. However, blaming the YSO filtering may amount to little more than a witchhunt. The expecation of a correlation may be premature, as the "high extinction ⇒ active star formation" argument may be too simplistic to reflect physical reality. In the pursuit of further insight, it will be worthwhile to repeat this analysis using several different YSO filtering criteria.

The lack of a correlation between YSO color and the mass of associated cores is also intriguing. The total remaining mass of a core seems to have little to do with the age of the stars it has produced. This raises questions about what prompts the collapse of a particular subregion; if mass is not a critical factor, it

may be that forces outside the core vitself play an important role, in a process of "triggered star formation". This mechanism has been proposed for Perseus previously; for example, see Kirk 2003.

In summary, the reddest YSOs in the [3.6μm]-[4.5μm] color space show definite clustering around 1.1mm and 850μm cores, with the tightest loci of red objects forming around 1.1mm objects. This YSO color property does not appear to show significant correlation with the basic physical properties of the nearest cores, including mass and extinction. To move explanations of this fact past the speculative stage, it will be necessary to repeat the analysis using a variety of definitions for "young stellar objects".

5 Star-Forming Efficiencies in Perseus

Previous sections of this paper were concerned with quantifying stellar distributions within Perseus, both absolute and relative to star-forming cores, and divided into subsets of age and region. This section moves on to a new, though related matter: how many stars are generated by a collapsing core? How "efficiently" does Perseus form stars?

This is not an easy question to answer. However, by making several simplifying assumptions, it is possible to make estimates of the efficiency using the COMPLETE and c2d data sets. The first assumption is that the 1.1mm and 850μm cores, as regions of peaking emissions, are the collapsing, gaseous cores involved in star formation. This allows us to identify the core mass as the star-forming mass in Perseus. The second assumption is that the motions of the YSOs are constrained to a degree that they are still located closer to their formative gas core (or cluster of cores) than to any other. This second assumption is perhaps unsound: mechanisms exist for accelerating stars to speeds as high as 20 km/s (Goodman 2004), but even with a velocity of 5 km/s, a million old star can travel over 5 pc! If Perseus is assigned an average distance from Earth of 250 pc (Enoch 2006), such a star could have over a degree of angular separation from its birthplace. Given the scale of the sub-regions in Perseus, this could be a serious problem. However, attempting to correct for such a problem is far beyond the scope of this analysis.

With these assumptions in hand, we can calculate a star-forming efficiency. Usually this quantity is a dimensionless number, found by taking the ratio of a region's stellar mass to its star-forming mass. As we do not have YSO mass estimates, we will instead calculate the ratio of a regions stellar *count* to its star-forming mass. This quantity will therefore have the unforunate units of $M_{\odot}^{-1}$. To distinguish this quantity from the usual star-forming efficiency, we will refer to it simply as ζ. To calculate ζ for a particular region, a center point was chosen, and the relevant ratio was calculated for a number of circular regions around the center point.

$$\zeta = \frac{\#stars}{cumulative\ core\ mass} \tag{4}$$

Chosing a center point is a somewhat dangerous game, as the decision greatly affects the calculations. Based on the usefulness of the extinction clumps in delimiting YSO clustering (§3.2), the centers of those cores were ultimately chosen as the central points.

Results for selected regions are presented in figures 19 and 20. The particular regions were selected based on their having enough stars to make an estimation of ζ statistically meaningful. Calculations were made at regular radial spacings out to the extinction clump's edge. The most striking feature of these plots are the strong differences between ζ for the 1.1mm and 850μm data. Each of the relevent studies (Enoch 2006 and Kirk 2006, respectively) used different criteria to define the edges of their cores - see §2.2 for details. These differences result in very different core masses, which of course cause the large separations between the curves. This makes direct comparison rather difficult, but at the same time, it is unreasonable to say that one method of core-definition is inherently better than the other. Therefore, this analysis will focus on the individual curves, or on morphological differences between the curves. Nevertheless, for the sake of completeness, a star-forming efficiency in each emission and for each region is presented in table 1. The number is based on the radius which contains 95% of the YSOs contained within the extinction clump.

Region	1.1mm ζ	850μm ζ
IC 348	4.16	25.5
NGC 1333	1.18	3.92
B1	0.26	1.60
L1455	0.38	6.11

Table 2: Values of ζ, based on the 95% of stars closest to the center of the relevant extinction clump. ζ is measured in units of inverse solar masses.

In general, the 1.1mm sources show approximately the same value of ζ regardless of how large an area is used in the calculation. There is some variation of course, but ζ varies by less than 1 in every cloud except IC 348. This anomaly is easily explained by a glance at figure 11; the stars in IC 348 are distributed somewhat widely around the extinction clump's center.

The 850μm data however, present a different pattern. There is much more spread in ζ depending on where the boundary is drawn, when compared to the 1.1mm. Part of this is due to the smaller number of 850μm cores than 1.1mm cores; the reduced counts within each radius introduce higher statistical fluctuations. However, even given these fluctuations, the 850μm data still shows an overall increase in ζ with increasing radial boundary - not just in IC 348, but in all four of the regions.

As the cumulative mass of the cores cannot be *de*creasing with radius, the only possibility is that the core mass is staying constant with radius as the number of stars is increasing (or, # stars is increasing faster than the cumulative mass). This has two implications. First, the 850μm cores are clustered more tightly than the 1.1mm. This can be visually confirmed by the Perseus-wide

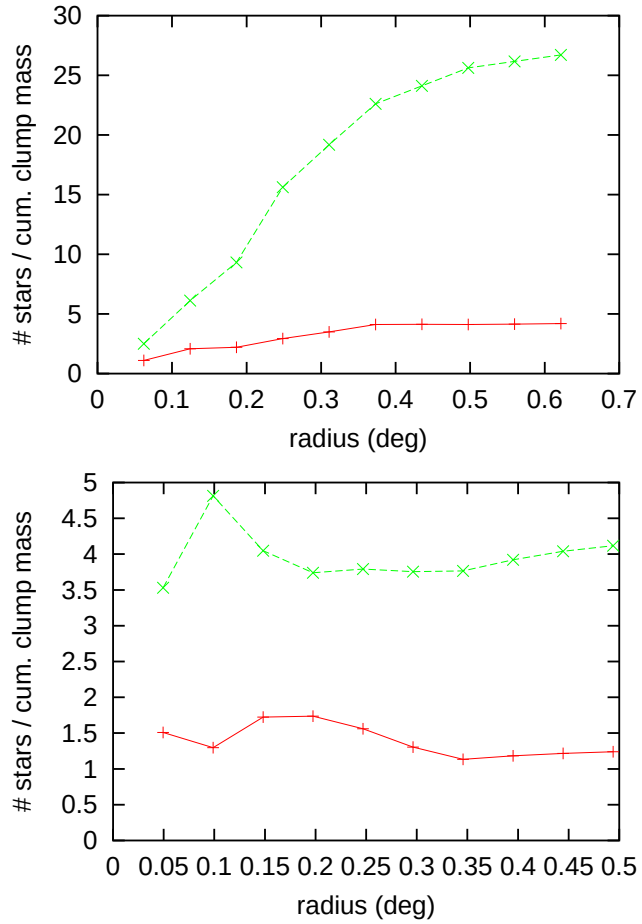

Figure 19: ζ, in units of $M_{\odot}^{-1}$, as measured for circular regions centered on the local extinction clump. Calculations are plotted for both 1.1mm (red) and 850μm (green) cores, in IC 348 (top) and NGC 1333 (bottom).

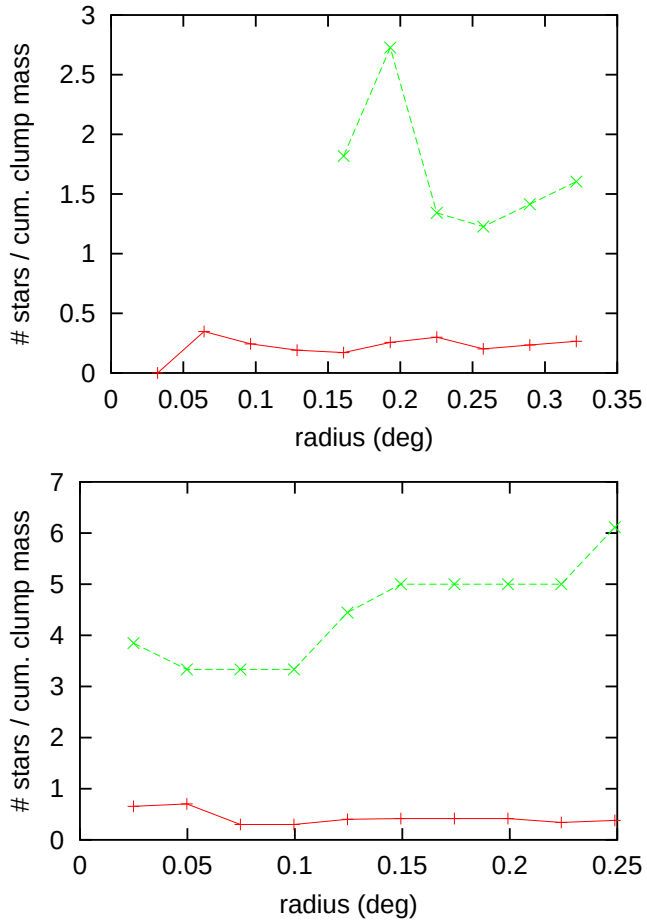

Figure 20: ζ, in units of $M_{\odot}^{-1}$, as measured for circular regions centered on the local extinction clumps. Calculations are plotted for both 1.1mm (red) and 850μm (green) cores, in B1 (top) and L1455 (bottom). Mass is measured in solar masses.

maps in §2. Second, and related to the first point, the 850μm star-forming mass is located at the *center* of YSO groups, while the 1.1mm star-forming mass is located *among* those groups.

At the same time, it is necessary to note that these results may be a function of observing technique, and not of the physical properties of the gas itself. The gaussian fitting used by the 1.1m survey is likely to break blobby filaments of gas into multiple regions. This can be seen in figure 6; note that a single 850μm core can often be associated with two or more 1.1mm cores. The 1.1mm emission really *may* be tracing different structures in the gas, but the diffuse nature of its cores could also be nothing more than an artifact of the gaussian fitting algorithms.

Thus, considering star-formation as a function of radius, rather than simply as a value, has unveiled an important distinction between the two surveys, as tracers of star formation. The existence of any distinction is intriguing, as the two surveys are intended to trace the same cores! The 850μm data summons an aesthetically pleasing picture of a central star-forming core, with its various progeny drifting outward from it. The 1.1mm data paints a sort of suburban landscape of star-formation, with YSOs developing in a relative spacious grid of cores, then drifting out to meet their neighbors.

6 Conclusion

6.1 Summary of Results

A combination of IRAC, 1mm, 850μm and 2μm observations of Perseus has produced several interesting features of star-formation in that cloud.

First, the young stellar objects show considerable self-clustering, with the tightest clustering associated with the youngest sources. 2μm extinction clumps turn out to be good outer bounds on this clustering.

Second, sources with reddened [3.6μm]-[4.5μm] color have a tendency to cluster around 1.1mm and 850μm emission peaks. The tightest clustering is associated with the 1.1mm cores. However, there appears to be little correlation between YSO color and the mass, flux, or local extinction of its nearest core neighbor.

Third, star-forming mass in Perseus show different distributions under the two tracers. The 1.1mm survey suggests that star-forming mass is well-spread, with pockets of formation distributed widely within larger regions of formations. The 850μm survey implies that star-forming mass is much more centralized.

6.2 Future Work

All of these findings are highly dependent upon the definition of the various objects involved. The 1.1mm and 850μm surveys define their cores very differently, which produces different counts and sizes for cores. A more detailed

study of these differences is called for.

The filtering criteria used to define YSOs also warrants further study. Repeating the above analyses with different YSO catalogs could help reveal which effects are physical, and which are simply products of selection biases in the filtering process. For example, allowing extended sources into the catalog might admit some class 0 objects; dropping the requirement that a YSO create a peak in all four IRAC bands might have the same effect.

The methods used to classify objects by infrared excess could also be tested by varying the color-color criteria used in these definitions. MIPS observations could provide a promising alternative.

ACKNOWLEDGEMENTS

First and foremost, I'd like to thank Professor Alyssa Goodman for all her help over this past year. I'd also like to thank Dr. Lori Allen for her assistance with the c2d data.

I am also indebted to the following members of the COMPLETE team for all the time they devoted to this project: Michelle Borkin, Paola Caselli, Jonathan Foster, Doug Johnstone, Jaime Pineda, Naomi Ridge, Erik Rosolowsky and Scott Schnee.

Finally, I would like to thank the Laxos and the Legends for their general excellence.

REFERENCES

Allen et al. 2004, ApJ, 154, 363.
Adams, F., et al. 1987, ApJ, 312, 788.
Andre, P. 1995, Aj&SS, 224, 29.
Carrol, B. & Ostlie, D. 1996. An Introduction to Modern Astrophysics (New York: Addison-Wesley), 437-476.
Enoch, M., et al. 2006, ApJ, 638, 293.
Evans et al. Third Delivery of Data from the c2d Legacy Project: IRAC and MIPS.
Foster, J. & Goodman, A. 2006, ApJL, 636, L105
Frink, S., et al 1997, A&A, 325, 613.
Goodman, A., & Arce,H. 2004, ApJ, 608, 831.
Harvey, P., et al. 2005, in prep.
Jorgensen et al. 2006, astro-ph/0603547.
Kirk, H., et al. 2006, astro-ph/0602089.
Lombardi M. & Alves, J. 2001, A&A, 377, 1023.
Peebles, P. 1980. The Large Scale Structure of the Universe (Princeton: Princeton U.), 143-144.
Ridge, N. et al. 2006, astro-ph/0602542.
Whitney, B., et al. 2003, ApJ, 598, 1079.
Williams, J., et al. 1994, ApJ, 428, 693.

Appendix A: Nearest Neighbors

This section contains a list of every YSO and its nearest core neighbors, both 1.1mm and 850μm.

NOTE: Extinctions are from the 2MASS survey, produced using the NICER algorithm.
NOTE: To conserve space, only a five star sample is shown here. The full list is available online at http://www.cfa.harvard.edu/COMPLETE/

KEY						
c2d	RA	dec	irac1	irac2	irac3	irac4
1mm	RA	dec	major axis	minor axis	rot. angle	extinction
850um	RA	dec	radius	extinction		
UNITS						
c2d	deg	deg	mag	mag	mag	mag
1mm	deg	deg	deg	deg	rad	Av
850um	deg	deg	deg	Av		
c2d	51.109699	30.521025	14.4326	13.4475	12.4779	11.368
1mm	56.9202	32.865898	0.0175	0.025278	-1.099557	7.56171
850um	51.341667	30.753611	0.009444	0.025278		
c2d	51.19096	30.219137	14.9787	13.9435	13.1016	11.9368
1mm	56.9202	32.865898	0.0175	0.025278	-1.099557	7.56171
850um	51.341667	30.753611	0.009444	0.025278		
c2d	51.331402	30.573374	12.502	11.7354	11.0606	10.1731
1mm	56.9202	32.865898	0.0175	0.025278	-1.099557	7.56171
850um	51.341667	30.753611	0.009444	0.025278		
c2d	51.413006	30.733032	12.502	9.5853	7.8242	6.6426
1mm	56.9202	32.865898	0.0175	0.025278	-1.099557	7.56171
850um	51.341667	30.753611	0.009444	0.025278		
c2d	51.535439	30.359343	13.3317	12.4791	11.7345	10.6875
1mm	56.9202	32.865898	0.0175	0.025278	-1.099557	7.56171
850um	51.341667	30.753611	0.009444	0.025278		

Appendix B: Star-Core Associations

This section contains a list of every YSO and its associated structure of cores. A core is assigned an association of type "1" if the YSO lies inside of its boundaries. A core is assigned an association of type "2" if its center lies within a core that has an association of type "1".

NOTE: Extinctions are from the 2MASS survey, produced using the NICER algorithm.
NOTE: To conserve space, only a five star sample is shown here. The full list is available online at http://www.cfa.harvard.edu/COMPLETE/

KEY							
c2d	RA	dec	irac1	irac2	irac3	irac4	
1mm	RA	dec	major axis	minor axis	rot. angle	extinction	asso. type
850um	RA	dec	radius	extinction	asso. type		

UNITS							
c2d	deg	deg	mag	mag	mag	mag	
1mm	deg	deg	deg	deg	rad	Av	
850um	deg	deg	deg	Av			

c2d	51.109699	30.521025	14.4326	13.4475	12.4779	11.368	
c2d	51.19096	30.219137	14.9787	13.9435	13.1016	11.9368	
c2d	51.331402	30.573374	12.502	11.7354	11.0606	10.1731	
c2d	51.413006	30.733032	12.502	9.5853	7.8242	6.6426	
1mm	51.4104	30.7328	0.014167	0.036667	-0.122173	7.56171	1
1mm	51.442051	30.7362	0.024167	0.037778	0.645772	7.56171	1
850um	51.408333	30.733055	0.008889	5.84966	1		
c2d	51.535439	30.359343	13.3317	12.4791	11.7345	10.6875	